J. Synchrotron Rad. (1996). **3**, 289–295

Protein Crystal Diffraction Patterns Using a Capillary-Focused Synchrotron X-ray Beam

D. X. Balaic,[a]* Z. Barnea,[a] K. A. Nugent,[a] R. F. Garrett,[b] J. N. Varghese[c] and S. W. Wilkins[d]

[a]School of Physics, University of Melbourne, Parkville, VIC 3052, Australia, [b]Australian Nuclear and Scientific Technology Organization, Private Bag 1, Menai, NSW 2234, Australia, [c]Biomolecular Research Institute, 343 Royal Parade, Parkville, VIC 3052, Australia, and [d]CSIRO Division of Materials Science and Technology, Locked Bag 33, Rosebank MDS, Clayton, VIC 3169, Australia. E-mail: dxb@physics.unimelb.edu.au

(*Received 14 January 1996; accepted 10 July 1996*)

A paraboloidally tapered glass monocapillary was used to focus an 8 keV monochromatized synchrotron bending-magnet X-ray beam into a 40 (±5) μm focal spot located 45 (±5) mm from the exit of the capillary. This focal spot had a measured intensity gain of 120 (±10) times the intensity present in an equivalent cross section of the unfocused beam from the monochromator. This focused beam was used to obtain oscillation diffraction patterns on image plates from a hen egg-white lysozyme protein crystal in two distinct geometries: one with the specimen crystal at the capillary exit and the other with the crystal at the beam focus. In the first geometry, focused Bragg reflections were observed at the focal plane. In the second geometry, diverging Bragg reflections of high intensity from a small crystal volume were observed. Image-plate diffraction patterns for these two geometries were compared with exposures with equivalent integrated diffracted intensities obtained using a 100 × 100 μm unfocused X-ray beam with the same crystal. The use of the focused beam resulted in a reduction in the exposure time required to produce equivalent patterns by a factor of between 70 and 100.

Keywords: protein crystallography; tapered capillary optics; X-ray focusing; X-ray optics.

1. Introduction

Macromolecular crystallography using synchrotron radiation is a well established and successful analytical method in the biological sciences for molecular structure determination of proteins and other large molecules. The high brilliance of synchrotron X-ray sources has reduced data-collection times from the days required with traditional laboratory X-ray sources to minutes, and has increased resolution. To achieve this, most protein crystallography beamlines that utilize synchrotron bending-magnet sources rely on some form of focusing mirror, curved crystal monochromator or a combination of the two to achieve a concentration of the available X-ray flux at the specimen position (Sakabe, 1991). This is necessary because the intensity available using a flat-crystal monochromator alone is insufficient to achieve both high resolution and acceptable signal-to-noise ratios in macromolecular diffraction data, even with large crystals. The long exposures required in this case either damage the crystal before high-angle data are obtained in the absence of cooling, or X-ray scatter from the cryostream imposes an unacceptable detector background if cooling is employed.

Tapered glass monocapillaries for use as X-ray beam intensifiers have been studied extensively in recent years (Stern, Kalman, Lewis & Lieberman, 1988; Engström, Larsson & Rindby, 1991; Engström, Fiedler & Riekel, 1995; Thiel, Bilderback & Lewis, 1993; Hoffman, Thiel & Bilderback, 1994). These optics utilize the total external reflection property of smooth glass surfaces for glancing angles of X-ray incidence (Henke, Gullikson & Davis, 1993). The intensity in a capillary output beam may be increased over that of the incident beam if the optic can either condense or focus the beam efficiently. The tapered glass capillary used in the experiments reported here differs from those reported by other groups in that its taper is paraboloidal, producing a geometrical focus of reflected X-rays at a point on the axis of the paraboloid for incident X-rays parallel to the capillary axis. Using such a capillary we have previously reported the first observation of focused X-rays beyond the exit aperture of a capillary optic (Balaic, Nugent, Barnea, Garrett & Wilkins, 1995). In this paper we report the first application of a paraboloidal capillary to macromolecular crystallography.

Our paraboloidally tapered capillaries are truncated 40 mm from the predicted geometrical position of the focal point to give an unobstructed beam focus with a converging incident focal beam. We define the 'working

* Author to whom correspondence should be addressed. D. X. Balaic is also associated with the CSIRO Division of Materials Science and Technology.

distance' of this optic as the distance between the exit end of the capillary and the focal point. We also adopt the term 'focal plane' to refer to the plane perpendicular to the beam axis that includes the focal point of the capillary. For ideal capillaries used with bending-magnet synchrotron sources, the diameter of the focal intensity FWHM can in principle be as small as 1 μm. In contrast, conical capillary tapers with small exit apertures are condensing (as opposed to focusing) optics within which the beam undergoes many reflections prior to its exit from the capillary. The narrowest point in the condensed beam from such a capillary is found at its exit aperture. Conical designs have previously provided intensity gains of the order of 10 in 10–100 μm diameter beam spots (Engström *et al.*, 1995) or gains of the order of 10^3 in submicrometer beam spots (Thiel *et al.*, 1993).

The particular paraboloidal taper profile chosen was calculated to give an optimal flux collection efficiency with respect to the cross-sectional area of incident beam intercepted and the variation of the glass surface reflectivity with X-ray energy and angle of incidence (Balaic & Nugent, 1995). The capillary was fabricated to these parameters using an automated system developed at the University of Melbourne.

2. Experimental procedure

The experiments were conducted on beamline 20B (the Australian National Beamline Facility), a bending-magnet beamline at the Photon Factory in Tsukuba, Japan. For this experiment the only optical element in the beamline was a single silicon (111) channel-cut monochromator which was set to provide 8 keV X-rays. The monochromator was slightly detuned to avoid the inclusion of higher-order X-ray harmonics. The resulting monochromatic beam was then apertured with slits to match the entrance aperture of the capillary, which was 1.2 mm in diameter. The 240 mm-long capillary was aligned with the X-ray beam axis using a pair of X–Y translation stages by observing the fluorescence pattern of the beam transmitted by the capillary on a ZnS screen placed 60 cm from the capillary exit. The observed pattern indicates optimal alignment of the capillary when a bright symmetrical ring is observed, centred about a bright spot. The bright ring corresponds to singly reflected focal rays diverging past the focus, and the bright central spot corresponds to the X-ray beam that passes through the capillary without reflection. By raster-scanning a 5 × 5 μm pinhole through the capillary-focused beam at various distances from the capillary, a focal region was found 45 (±5) mm beyond the capillary exit (Fig. 1).

The diameter of the exit aperture of the capillary was 0.5 mm, yielding a (maximum) convergence angle at the focus of 11 (±1) mrad. It should be noted that 14% of the beam that enters the capillary will proceed directly through the exit aperture without reflection. This collimated portion of the incident beam (visible as a 500 μm diameter disc of low intensity in Fig. 1) makes little contribution to the focal region, which is dominated by the intensity in the focal peak. The absence of significant X-ray intensity outside the region of the disc in Fig. 1 indicates that parasitic scatter from the capillary is negligible. The focal FWHM of this capillary was 40 (±5) μm and this region received 120 (±10) times the intensity present in the incident beam. The maximum intensity observed within the focal peak corresponded to an intensity gain of 700 (±50) in an area of 5 × 5 μm. As the incident X-rays are highly parallel, the collimated portion of the incident beam may be removed with no loss of focusing efficiency. This may be achieved by placing a stop at the centre of the entrance aperture of the capillary, with the stop diameter equal to the exit aperture of the capillary. Such a stop was not employed in the experiments reported here.

The crystal used for the diffraction experiments was a hen-egg lysozyme protein crystal, which has a tetragonal structure ($P4_32_12$) with unit-cell dimensions $a = b = 79.1$ Å and $c = 37.9$ Å (Blake *et al.*, 1965). This protein was selected for use in these experiments due to its strong diffraction characteristics and imperviousness to long X-ray exposure without cooling. Both of these features were necessary to demonstrate acceptable diffraction patterns using the unfocused monochromatic beam at the beamline

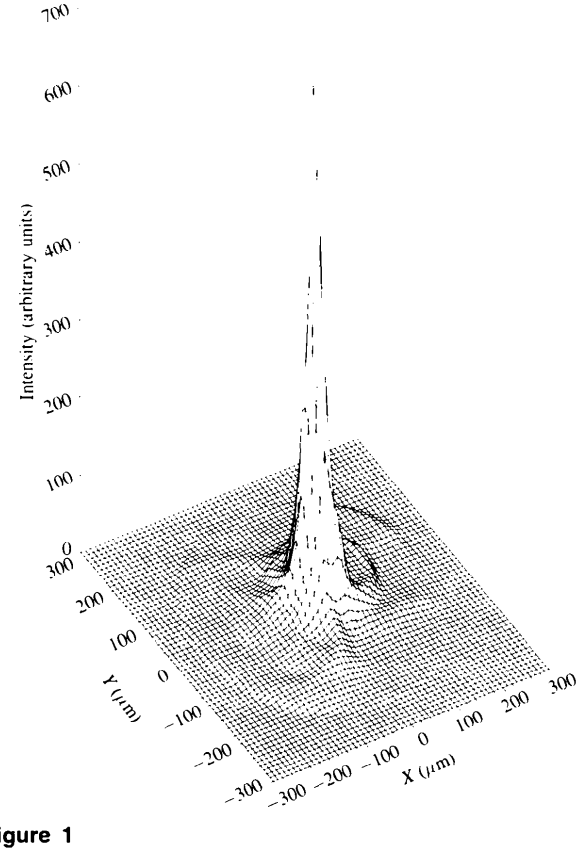

Figure 1
Capillary beam focus intensity distribution. The X and Y axes are perpendicular to the beam axis. The intensity axis has been scaled so that the unfocused beam from the monochromator has unit intensity. The unfocused beam can be seen as a 500 μm disc of low intensity centred on the focal peak in this plot.

used for these experiments. The crystal resembled a four-sided pyramid, with a 450 × 500 μm base and a peak height of 200 μm. It was aligned with its peak towards the capillary and its flat base towards the image plate. The 20 × 25 cm image plate was placed 5 mm above the beam axis. The image plates were scanned using a Fuji BAS image-plate scanning system with 120 μm resolution to produce 100 μm pixels with 256 logarithmic intensity levels corresponding to four orders of magnitude of dynamic range.

Image-plate exposures of the protein crystal diffraction pattern were first obtained using the unfocused beam from the monochromator apertured to 100 × 100 μm using slits. Exposure times were optimized in the unfocused beam exposures to achieve near-saturation of the lowest-order reflections on the image plate for a single 2° rotation of the crystal about the horizontal axis, which coincided with the *a* axis of the crystal. X-ray diffraction patterns were then obtained from the protein crystal using the capillary-focused beam. Exposure times using the capillary were adjusted to produce equivalent integrated spot intensities to the unfocused beam exposures for a comparable range of reflections and (approximately the same) single 2° rotation of the crystal.

Two capillary crystal geometries were investigated. In the first (Fig. 2) the crystal was placed 5 mm from the exit aperture of the capillary and an image plate was placed at the focal plane (focused reflection geometry). In the second (Fig. 3) the crystal was placed at the capillary beam focus and the image plate at various positions beyond the beam focus (diverging reflection geometry). Owing to constraints of stage positioning it was necessary to rotate the crystal by 10° about the vertical axis for the focused reflection geometry experiments. This resulted in the two sets of patterns being obtained for different crystal orientations.

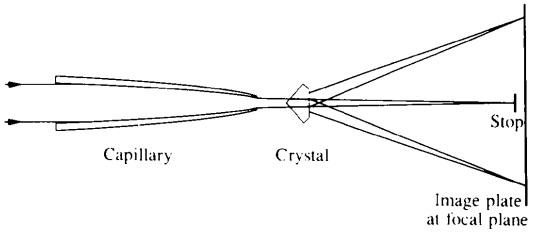

Figure 2
Tapered capillary with protein crystal at the capillary exit and image plate at the focal plane (focused-reflection geometry).

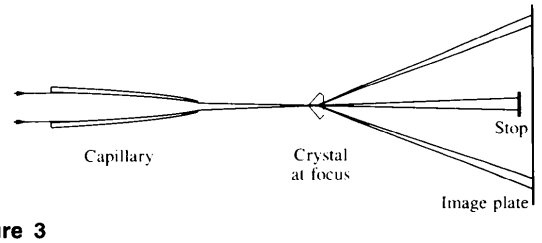

Figure 3
Tapered capillary with protein crystal at the beam focus and image plate beyond the beam focus (diverging-reflection geometry).

All exposures were carried out at room temperature in air as the crystal-to-plate distances were small.

The dimensions of the 100 × 100 μm unfocused beam were chosen for several reasons. Firstly, this beam produced reflection spots with intensity FWHM comparable with the focused Bragg reflections observed in the focusing geometry. Secondly, the 100 × 100 μm beam cross section was similar to the focused beam cross section at the crystal in the diverging reflection geometry. Finally, a small-diameter beam is necessary to reduce image-plate background due to air scatter from the incident beam over the long exposure times required with the unfocused beam. Also, a beam size of 100 × 100 μm is commonly used at synchrotron protein crystallography stations for high-resolution work, even with large crystals which are irradiated piecewise.

3. Results

Excellent diffraction patterns were obtained using both the focused reflection geometry and the diverging reflection geometry (Figs. 4*a*, 7*a*). For equivalent diffraction pattern integrated intensities, exposures with the capillary-focused beam in either diffraction geometry were between 70–100 times shorter than those obtained with the 100 × 100 μm unfocused beam. This result is in good agreement with the previously measured intensity gain in the focal FWHM of 120 (±10) times the intensity of the unfocused X-ray beam. Such a comparison of the focused-beam diffraction patterns with the previously determined gain of the capillary is fully justified because in the focused-beam case the crystal intercepts the entire beam, whilst in the unfocused-beam case the beam intensity (flux per unit area) remains the same whatever the beam cross section.

The observed background intensity, due mainly to air scatter, is low in both the capillary-focused beam and the 100 × 100 μm collimated beam diffraction patterns. Fig. 5 shows the variation of integrated-intensity-to-background ratio as a function of total observed intensity for a range of observed reflections from each experiment. The reflections used in this diagram cover the observed range of intensities and 2θ angles in each pattern. The integrated-intensity-to-background ratios from the capillary-focused beam are seen to be systematically and significantly higher than those from the collimated beam. This is to be expected in view of the longer exposures required with the collimated beam. The patterns obtained with exposures differing by two orders of magnitude are seen to exhibit comparable diffraction intensities.

The focused reflection geometry produced the first observation of focused Bragg reflections using a tapered capillary optic. In the focusing geometry the entire crystal is exposed to the beam at the capillary exit and the Bragg reflections are observed at the capillary focal plane. The focused Bragg reflections were observed to have a FWHM of approximately 100 μm. In the focused reflection geometry, diffraction patterns from the protein crystal were

obtained with exposures of 2 s per degree of rotation. The highest d-spacing observed from the lysozyme crystal in the focused reflection geometry was 2.5 Å [$(\sin\theta)/\lambda$ = 0.2 Å^{-1}], achieved within 10 s per degree of rotation. The equivalent image-plate exposure with a 100 × 100 μm unfocused beam required 200 s per degree of rotation.

A 50 s per degree image-plate exposure with the crystal fully illuminated by the unfocused beam produced diffraction spots of at least 300 μm FWHM, for all observable orders (inset, Fig. 4*b*). This exposure did not produce integrated diffraction spot intensities equivalent to those obtained with the capillary before background scatter saturated the image plate. The inset to Fig. 4(*b*) has had the background subtracted and contrast enhanced to provide a spot-size comparison with the main figure. Figs. 4(*a*) and 4(*b*) have not had any background subtracted.

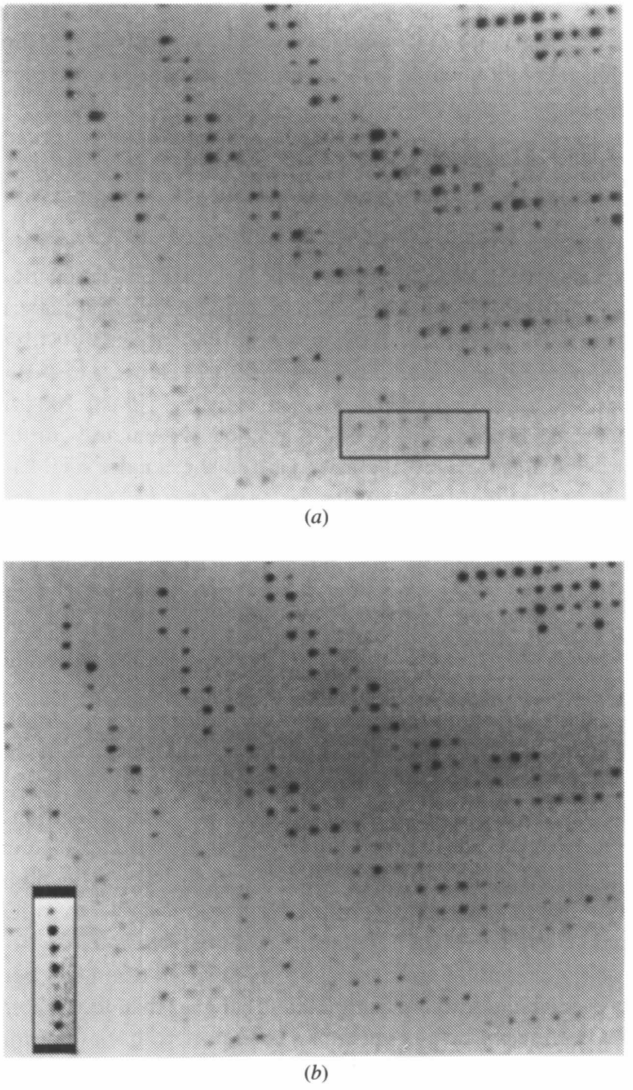

Figure 4
Detail of image-plate protein crystal diffraction patterns for (*a*) a capillary-focused incident beam in focused-reflection geometry with the crystal positioned 5 mm from the capillary exit, and (*b*) an unfocused 100 × 100 μm incident beam. In both cases the image plate is 37 mm from the crystal and monochromatic 8 keV (1.54 Å) X-rays are used. The crystal was rotated over 2° with exposure times of (*a*) 2 s per degree, and (*b*) 200 s per degree. The inset to pattern (*b*) shows the equivalent image-plate spot size when the entire crystal is illuminated by the unfocused beam (50 s per degree exposure, background scatter subtracted). The regions shown are between 3 and 10 Å [$(\sin\theta)/\lambda$ = 0.05–0.16 Å^{-1}]. Sections of image plates shown cover 25 × 20 mm.

In the focused reflection geometry the focal spot size of the capillary-focused beam and the crystal mosaic spread together place a limit on the resolution of Bragg reflections at the focal plane of the capillary. The crystal mosaicity convolves with the beam convergence to produce the actual spot size on the surface of a 'focal sphere' centred on the crystal. This sphere has a radius equal to the capillary working distance less the distance between the crystal and the capillary. The distance between the surface of the focal sphere and the focal plane increases with the Bragg angle, so that high-angle reflections will be less focused when observed at the focal plane. This problem is addressed in two ways. Firstly, the depth of field of the beam focus (~±5 mm for the capillary used in these experiments) partially compensates for the relative error in the locations of the focal plane and focal sphere. Secondly, the plane of observation may be moved closer to the crystal to improve the resolution of high-angle reflections, at the expense of defocusing some low-angle reflections.

For two adjacent Bragg reflections to be resolved, we may adopt a resolution criterion that requires resolved reflections to be separated by, for example, more than the sum of their respective radii. Then, taking $\tan\theta \simeq \theta$, we may define the resolution criterion for this geometry as

$$\theta_{ab} > w/l + \sigma,$$

where w is the focal spot FWHM, l is the working distance of the capillary, σ is the angular mosaic spread of the

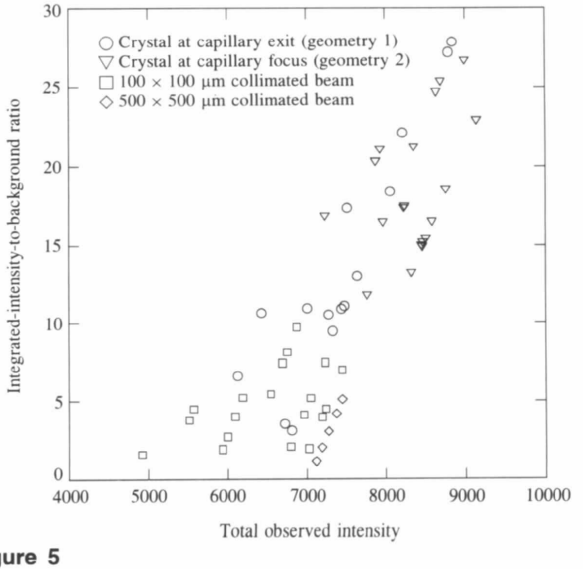

Figure 5
Diffraction pattern integrated-intensity-to-background ratio variation with total observed intensity (including background) for the capillary and collimated beam diffraction experiments. The integrated spot area in each case is 7 × 7 100-μm pixels.

crystal, and θ_{ab} is the angle between the two highest-order Bragg reflections to be resolved.

If a stop is not employed to remove the collimated portion of the output beam from the capillary, then the crystal will also diffract this component of the beam. At the focal sphere, the corresponding diffracted beam will be observed as a disc of low-intensity X-rays centred on the focused Bragg reflection. Although this diffracted beam will be approximately 100 times less intense than the focused Bragg reflection, its lateral extent will be at least equal to the diameter of the incident beam intercepted by the crystal. The resulting intensity distribution in the reflection spots will resemble the intensity distribution in Fig. 1 convolved with the angular mosaic spread of the crystal. This situation is best avoided in the focused reflection geometry as it would reduce the resolution of the diffraction spots on the focal sphere.

The spacing of the Bragg reflection peaks in Fig. 4(*a*) may be used to calculate the maximum crystal cell-edge resolution possible with this capillary in this geometry. Fig. 6 shows a contour plot of a set of reflections from the region at a *d*-spacing of ~3 Å shown boxed in Fig. 4(*a*). The contours shown represent five level increments in the (decimal logarithmic) intensity scale of the scanned image-plate pixels. The lowest contour shown is within two levels of average background intensity. Using the observed reflection spot separation in this diagram and the unit-cell edge of the lysozyme crystal, we calculate that this capillary could produce resolved Bragg reflections in this geometry from a crystal with a unit-cell edge of 182 ± 8 Å and mosaic spread of 0.3°. This cell-edge resolution can be improved by removing the collimated portion of the output beam from the capillary, as described above.

In diverging reflection geometry the X-ray beam is focused into a small volume of the crystal. The resultant diffraction pattern will not exhibit overlap of adjacent Bragg reflections where the resolution condition given below is satisfied, regardless of crystal-to-image-plate distance. Fig. 7 compares a 2 s per degree diverging reflection geometry exposure of the lysozyme crystal with a 100×100 μm unfocused beam exposure of 200 s per degree (no background removed in either exposure). The highest *d*-spacing observed from the lysozyme crystal in this geometry was 2.5 Å, for 10 s per degree exposures. The spot size increased slowly with increasing crystal-to-image-plate distance and this offers a useful means of adjustment of spot size to match image-plate scanning resolution criteria. In these image-plate exposures the observed spot

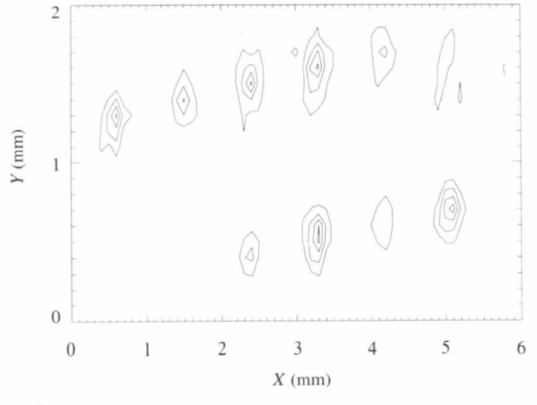

Figure 6
An intensity contour plot corresponding to the section of Fig. 4(*a*) shown boxed. The contour interval is five logarithmic intensity levels. The lowest contour shown is within two levels of background. The region shown corresponds to a crystal *d*-spacing of ~3 Å.

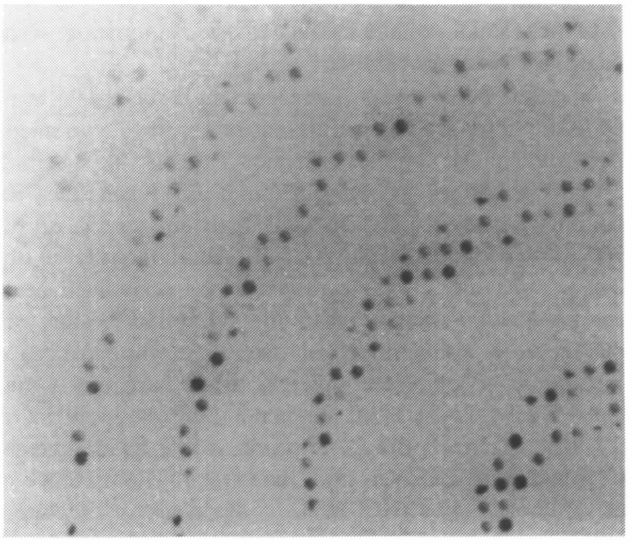
(*a*)

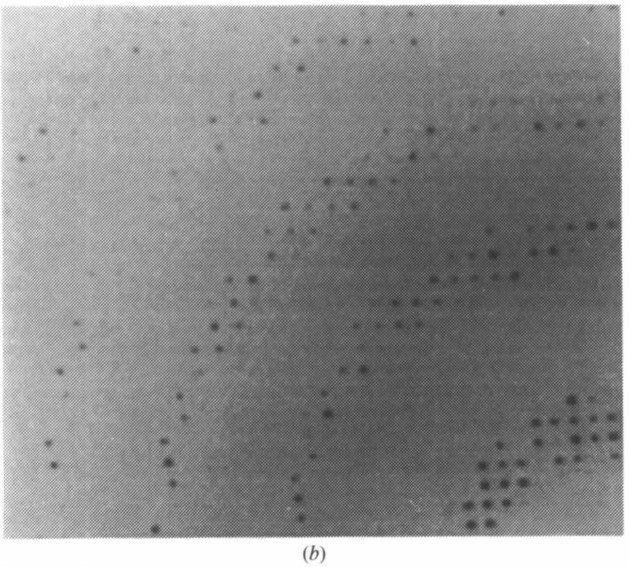
(*b*)

Figure 7
Detail of image-plate protein crystal diffraction patterns for (*a*) a capillary-focused incident beam in diverging-reflection geometry (crystal at the beam focus), and (*b*) an unfocused 100×100 μm incident beam. The image-plate-to-crystal distances were 51 mm in (*a*) and 37 mm in (*b*). In each exposure monochromatic 8 keV (1.54 Å) X-rays were used. The crystal was rotated over 2° with exposure times of (*a*) 2 s per degree, and (*b*) 200 s per degree. The regions shown are between 3 and 10 Å [$(\sin\theta)/\lambda = 0.05$–$0.16$ Å^{-1}]. Sections of image plates shown cover (*a*) 35×30 mm, and (*b*) 25×21.5 mm.

divergence was calculated to be 12 (±1) mrad. We may also define a resolution criterion for this geometry to be

$$\theta_{ab} > \alpha + \sigma,$$

where α is the maximum angle of convergence in the capillary-focused beam, σ is the angular mosaic spread of the crystal, and θ_{ab} is the angle between the two highest-order Bragg reflections to be resolved. Reflections satisfying this criterion will be resolved at all image-plate distances from the crystal. Owing to the high concentration of intensity in the focus, the diverging reflection geometry makes it possible to obtain diffraction patterns from extremely small protein crystals whose examination would otherwise be impracticable.

The presence of the collimated beam in the output beam from the capillary has a different effect in this geometry from that in the focused reflection case. If the specimen crystal is similar in size to the beam focus then the collimated portion of the beam largely misses the crystal and so contributes negligible diffracted intensity to the Bragg reflections. If the crystal and the collimated beam are comparable in size then the diffracted beams will include an intensity component due to the collimated beam. This intensity component diverges much more slowly than the diffracted focal beam component and thus remains at the centre of each Bragg reflection as the latter diverges with increasing distance from the crystal. The presence of the collimated and focal beam components in the Bragg reflections imposes a further constraint upon the resolution criterion given above. The resolution criterion will only apply beyond a minimum distance of observation from the crystal corresponding to the distance required for the focal component of the diffracted beam to diverge sufficiently so that it completely overlaps the collimated beam component of each reflection. This condition may be stated as

$$D > s/\alpha,$$

where D is the minimum radial observation distance from the crystal, s is the diameter of the crystal illuminated by the collimated beam from the capillary, and α is the maximum angle of convergence in the capillary-focused beam.

Fig. 8 shows Bragg reflections from the lysozyme crystal in diverging reflection geometry, observed 135 mm from the crystal. The reflections have diverged sufficiently for the collimated beam component to be observable in each reflection as a central spot surrounded by a discrete ring of intensity corresponding to the diverging focal beam component. Although it is unnecessary to observe reflections at such large distances from the crystal, the fact that different reflections remain identical in shape and structure with increasing distance from the crystal suggests that the focused beam is being diffracted over a similar angular range in each reflection.

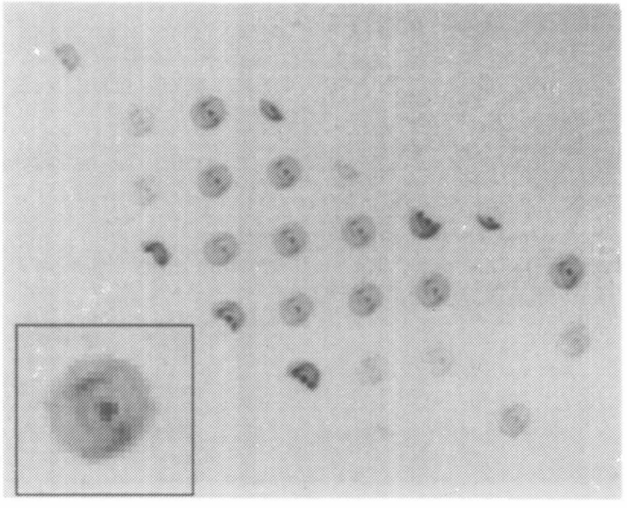

Figure 8
Detail of an image-plate protein crystal diffraction pattern for an incident capillary-focused beam in diverging-reflection geometry (crystal at the beam focus). The image plate is 135 mm from the crystal and monochromatic 8 keV (1.54 Å) X-rays are used. The diffraction spots are approximately 1.5 mm in diameter. The calculated diffraction spot divergence is 12 (±1) mrad. The inset shows a diffraction spot at 3× magnification. The crystal was rotated over 2° for an exposure time of 10 s per degree. The region shown lies between 6.4 and 8.6 Å [$(\sin\theta)/\lambda$ = 0.058–0.078 Å^{-1}]. The section of the image plate shown covers 30 × 24 mm.

4. Discussion

The results presented in this paper suggest several novel possibilities for crystallography performed with capillary-focused X-ray beams. These include:

(*a*) Diffraction from very small crystals or individual regions of multi-domain, non-uniform or plate crystals. The beam focus diameter (40 ± 5 µm FWHM) contains 120 (±10) times the intensity of the unfocused beam from the monochromator, permitting analysis of crystals or regions of equivalent size within reduced exposure times. It is also worth noting that the intensity distribution within the focal FWHM is sharply peaked, with a measured maximum intensity of 700 (±50) times that in the unfocused beam in an area of 5 × 5 µm at the centre of the beam. This may permit study of extremely small crystals within a reasonable exposure time.

(*b*) For sufficiently large crystals, the focused reflection geometry permits the collection of data in the focal plane close to the crystal. In this case the spot size is given by the convolution of the focal spot FWHM with the crystal angular mosaic spread parameter. The compact area occupied by the diffraction pattern permits the use of a small-aperture high-resolution detector, *e.g.* direct exposure or phosphor-coupled CCD detector (Bilderback, Thiel, Pahl & Brister, 1994).

(*c*) The diverging reflection geometry permits matching of both detector resolution and aperture with diffracted spot dimensions at no cost in structure resolution, as diffracted spots satisfying the resolution criterion remain resolved at all distances from the crystal. The diffracted spots remain round and symmetrical irrespective of image-plate position, allowing for ready integration over their extent in any image

plane chosen. Once again the resolution criterion given above for this geometry specifies the maximum capillary-beam convergence angle permitted for resolution of Bragg reflections from a crystal of given mosaicity.

(*d*) For crystals with a very large mosaic spread the resolution criteria given above may not be satisfied in either geometry to achieve resolution at a desired *d*-spacing. In this case the resolution criteria may be applied in reverse to specify the design of a capillary with a narrower focal convergence angle (with a corresponding decrease in available focal intensity) to be used for diffraction studies of a crystal with a given mosaic spread.

(*e*) The diverging reflection geometry permits the piece-wise irradiation of a crystal larger than the focal spot size, so that more diffraction data may be collected from particularly radiation-sensitive crystals by using different regions of the crystal for additional exposures (Sakabe, 1991).

(*f*) The two geometries discussed in this paper are by no means mutually exclusive. A continuum of experimental configurations between these extremes is possible, with prospective advantages for particular crystals and/or detection schemes.

(*g*) Although the capillary will demonstrate some decrease in transmission efficiency with increased X-ray energy (Balaic *et al.*, 1995), the focal position and focal spot size are essentially independent of X-ray energy. The capillary may thus also be used as an achromatic optical element of high efficiency for white-beam Laue photography, with the added possibility of time-resolved studies due to the short exposure times necessary to collect data.

(*h*) The substantial working distance (40–50 mm) available with focusing capillaries of the design described in this paper facilitates their use in diffraction experiments involving cryo-cooling, heat, pressure or complex instrumentation at the specimen position (Bilderback *et al.*, 1994).

(*i*) The focusing characteristics of the paraboloidally tapered capillary are optimal for highly parallel X-ray beams. However, this does not preclude the use of such optics with laboratory sources employed in conjunction with monochromator crystals or mirror optics that produce beams of low divergence. Although the greater beam divergence incident at the capillary will increase the FWHM of the beam focus, considerable intensity gain and focusing are nevertheless achievable.

5. Conclusions

The use of a capillary-focused monochromatic X-ray beam for protein crystal diffraction has been demonstrated. Two distinct diffraction geometries were investigated: the focused reflection geometry in which the crystal is positioned at the capillary exit, and the diverging reflection geometry in which the crystal is positioned at the beam focus. Using the first geometry, focused Bragg reflections were observed for the first time using a capillary optic. An exposure-time reduction of between 70 and 100 was achieved when compared with equivalent image-plate exposures using an unfocused 100 × 100 μm monochromatized synchrotron beam. A similar reduction of exposure time was demonstrated using the diverging reflection geometry. This geometry also permits diffraction from a small volume of crystal. Reflections down to a resolution of 2.5 Å were observed in image-plate exposures from single 2° crystal rotations of 10 s per degree using the focused beam in both diffraction geometries.

The authors wish to acknowledge the support of this work by an ARC Small Grant from the Australian Research Council, ANSTO for continued access to the Australian National Beamline Facility at the Photon Factory, and a CSIRO postgraduate studentship held by DXB.

References

Balaic, D. X. & Nugent, K. A. (1995). *Appl. Opt.* **34**, 7263–7272.
Balaic, D. X., Nugent, K. A., Barnea, Z., Garrett, R. F. & Wilkins, S. W. (1995). *J. Synchrotron Rad.* **2**, 296–299.
Bilderback, D. H., Thiel, D. J., Pahl, R. & Brister, K. E. (1994). *J. Synchrotron Rad.* **1**, 37–42.
Blake, C. C. F., Koenig, D. F., Mair, G. A., North, A. C. T., Phillips, D. C. & Sarma, V. R. (1965). *Nature (London)*, **206**, 757–761.
Engström, P., Fiedler, S. & Riekel, C. (1995). *Rev. Sci. Instrum.* **66**, 1348–1350.
Engström, P., Larsson, S. & Rindby, A. (1991). *Nucl. Instrum. Methods*, A**302**, 547–552.
Henke, B. L., Gullikson, E. M. & Davis, J. C. (1993). *At. Data Nucl. Data Tables*, **54**, 2.
Hoffman, S. A., Thiel, D. J. & Bilderback, D. H. (1994). *Nucl. Instrum. Methods*, A**347**, 384–389.
Sakabe, N. (1991). *Nucl. Instrum. Methods*, A**303**, 448–463.
Stern, E. A., Kalman, Z., Lewis, A. & Lieberman, K. (1988). *Appl. Opt.* **27**, 5135–5139.
Thiel, D. J., Bilderback, D. H. & Lewis, A. (1993). *Rev. Sci. Instrum.* **64**, 2872–2878.